Electrochimica Acta 160 (2015) 227–234

Contents lists available at ScienceDirect

Electrochimica Acta

journal homepage: www.elsevier.com/locate/electacta

Comparative studies of pyridine and bipyridine ruthenium dye complexes with different side groups as sensitizers in sol-gel quasi-solid-state dye sensitized solar cells

D. Sygkridou [a,b], C. Sahin [c,**], C. Varlikli [d], E. Stathatos [a,*]

[a] Electrical Engineering Department, Technological-Educational Institute of Western Greece, 26334 Patras, Greece
[b] Physics Dept., University of Patras, 26500 Patras, Greece
[c] Chemistry Department, Art & Science Faculty, Pamukkale University, Denizli, Turkey
[d] Solar Energy Institute, Ege University, 35100-Bornova, Izmir, Turkey

ARTICLE INFO

Article history:
Received 17 October 2014
Received in revised form 8 January 2015
Accepted 30 January 2015
Available online 7 February 2015

Key words:
ruthenium(II) complexes
quasi-solid-state electrolyte
hybrid organic inorganic materials
dye-sensitized solar cells

ABSTRACT

Six ruthenium(II) complexes as charge-transfer sensitizers for dye sensitized solar cells (DSSCs) are synthesized. The absorption and electrochemical properties of newly synthesized ruthenium-dye molecules contained one bipyridine (bpy) ligand with two carboxylic groups have been investigated. Among them, four ruthenium(II) complexes contain a second bpy ligand with branching and non-branching side groups containing C and H only and the remaining two ruthenium(II) complexes instead of a second bipyridine (bpy) ligand, they consisted of a pyridine (py) ligand with side groups containing –C–O–C–molecular group. Dye sensitized solar cells employing quasi-solid state electrolyte and the six ruthenium complexes are constructed and electrically characterized under standard conditions of light irradiance (1000 W/m^2, AM 1.5). Their behavior is compared with that of commercially available ruthenium complex D907 in terms of current-voltage characteristic curves under simulated light and dark while electrochemical impedance spectroscopy showed comparable results for local resistance to charge transfer across the TiO_2-electrolyte interface and free electron lifetimes for two bipyridine and commercial D907 complexes. The influence of molecular side groups into ruthenium-dye molecules is discussed in terms of the cells' efficiency.

1. Introduction

Since the first report on dye-sensitized solar cells (DSSCs) introduced by M. Grätzel at 1990 [1], too much attention has been attracted to the development of new and ever more performing materials as this technology fulfils many requirements concerning the cost of the materials and cells, low energy expenditure and ease of preparation [2–5]. Their maximum conversion efficiency of over 12 percent [6] suggests that they are a promising type of next generation solar cells. For their commercial application, it is important to develop low-cost materials and to achieve maximum efficiency for the cells. The components of a DSSC have more or less been standardized and they are: a TiO_2 nanocrystalline film deposited on a SnO_2:F transparent conductive electrode (negative electrode), a ruthenium bipyridyl derivative adsorbed and chemically anchored on TiO_2 nanocrystallites, an electrolyte bearing the I^-/I_3^- redox couple and a platinized SnO_2:F electrode (positive electrode). A large volume of the recent works on DSSC's is devoted to the study of the physicochemical state of the electrolyte [7–9]. This is dictated by some concern that has been expressed as to the long term photochemical stability of the devices due to leakage of the electrolyte caused sealing problems as well as stability and durability of liquid electrolytes. However, one more critical factor for better cell performance is the optimization of dye sensitizer in terms of increasing light-harvesting capability, improving charge transport and reducing recombination of excited electrons. In general, after irradiation of the solar cell, light is absorbed by the dyes' molecules that are anchored on the TiO_2 surface and the electrons are injected from the excited state of dye into the conduction band of the

* Corresponding author. Department of Electrical Engineering, Technological-Educational Institute of Western Greece, GR-26334 Patras, Greece. Tel.: +30 2610 369242; fax: +30 2610 369193.
** Corresponding author. Chemistry Department, Art & Science Faculty, Pamukkale University, Denizli, Turkey Tel.: +90 2582963526; fax: +90 2582963535.
E-mail addresses: cigdemsahin82@gmail.com (C. Sahin), estathatos@teipat.gr (E. Stathatos).

http://dx.doi.org/10.1016/j.electacta.2015.01.195
0013-4686/

semiconductor film. At the same time, the dyes are regenerated by the redox mediator in the electrolytic solution to provide efficient charge separation. Therefore, a considerable degree of energy conversion efficiency of a solar cell depends on the dye used and the collaboration between these molecules and the electrolyte making this a critical factor for the optimization of cells' efficiency and overall performance. Various sensitizers have been proposed in the past and their performances were investigated during the past two decades [10–14]. These are separated in two major categories. The first is related to the pure organic dyes prepared according to cheap synthetic routes or obtained from nature as component of flowers and fruits [15–17]. The reason for choosing pure organic dyes is that they have certain advantages over metal based photosensitizers; they are easily modified with common synthetic procedures while they exhibit high molar extinction coefficients compared to metal complexes [18]. Organic dyes with high molar extinction coefficients could be advantageously used in thin titanium dioxide film based solar cells which are mainly required in solid state devices where the mass transport and pore filling are limited affecting the performance of the cells. However, the overall performance obtained for DSSCs comprising pure organic dyes is not competitive, while their stability is limited after several hours of continuous illumination. In the second category transition coordination complexes (Ru-polypyridyl complexes) are employed as charge-transfer sensitizers, harvesting higher than 11% solar-to-electric energy conversion [19,20]. These complexes are also one of the most effective sensitizers because of their high efficiency, excellent chemical stability, favorable photoelectrochemical properties, and intense charge transfer absorption in wide visible range. Numerous reports of ruthenium(II) complexes with different ligands have been published with an aim to improve the device efficiency and stability. In general, these dyes are assembled by incorporation of bipyridines and thiocyanate ligands. The recent research in ruthenium sensitizers is focused on structure modification of the ligands to improve light harvesting, electron injection efficiency and finally the efficiency of the DSSCs [21,22]. In particular, modifications of ancillary ligands allowed a record efficiency of 12.3% for Z991 dye, which is an N3 analogue with an ancillary ligand substituted with bithiophene containing moieties [19]. Ligand modifications could also contribute to the better collaboration among ruthenium dye molecules and electrolytes intermittently used in DSSCs especially in the case that quasi-solid state electrolytes are used.

In this work, we explore the influence of molecular side groups on the performance of DSSCs based on quasi-solid state electrolyte. In particular, the choice of these structures was made on our basic aim to provide a possible solution to the two of general problems appearing in DSSCs technology based on ruthenium complexes. Those are addressed as, solubility of the dye that may cause aggregation of the dye on TiO_2 surface, and water adsorption of the dye that affects the performance of the cell. The different alkyl substituent of the synthesized complexes may provide enhancement on both of them. Spectroscopic, and electrochemical characterizations for the six as-prepared ruthenium complexes are presented while the electrical characterization of DSSCs obtained with these dyes are also presented in comparison with that achieved with a commercial D907 - (Everlight, Taiwan) ruthenium dye which is a dye molecule with similar structure as the new ruthenium(II) complexes.

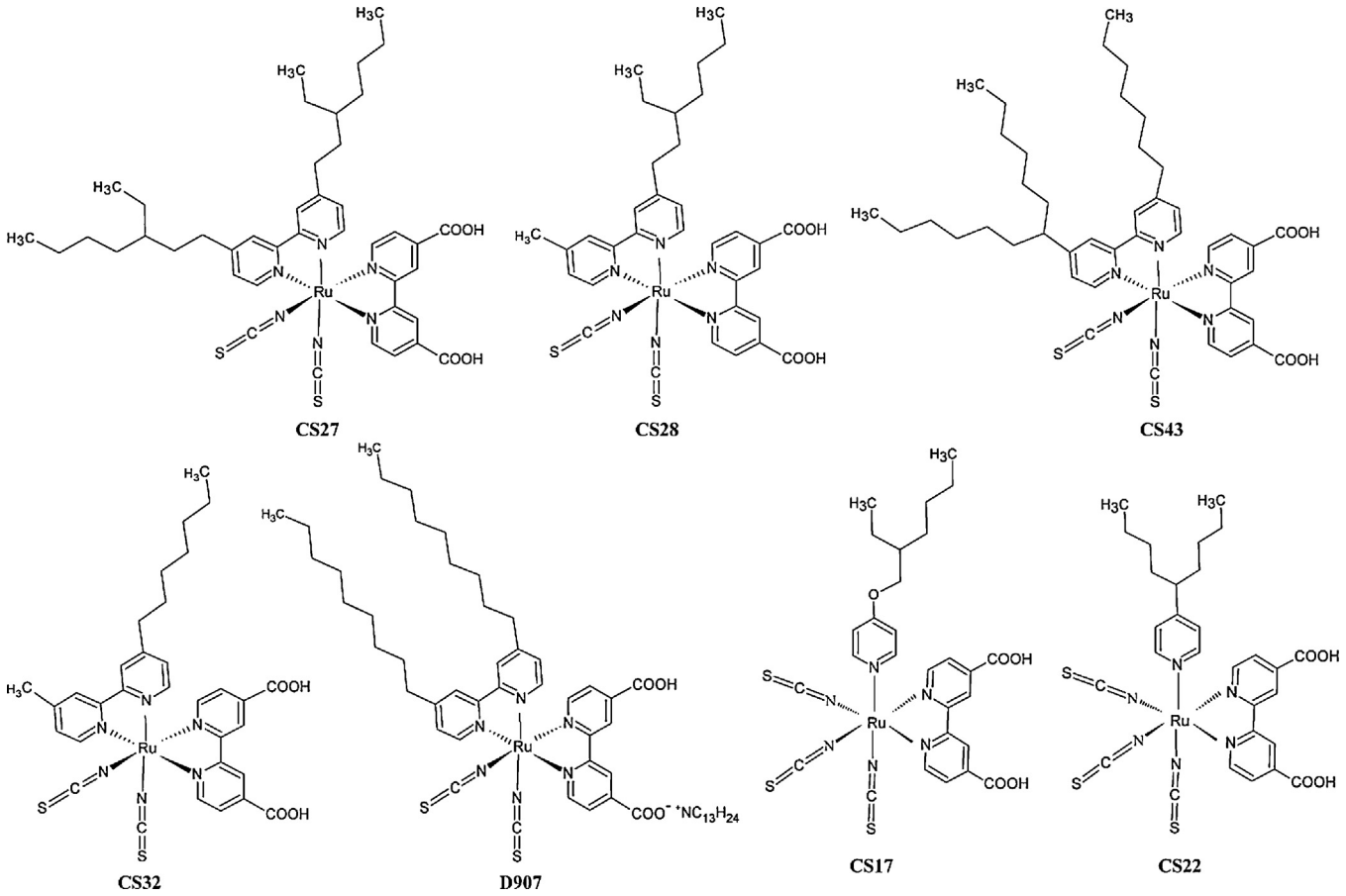

Scheme 1. Molecular structures of the ruthenium(II) complexes.

2. Experimental Section

2.1. Materials

2.1.1. Materials for new dye complexes synthesis

Dichloro(*p*-cymene) ruthenium(II) dimer, tetrabutyl ammonium hexafluorophosphate ($TBAPF_6$), ammonium thiocynate, 1-bromohexane were provided from Fluka. Chromium(VI) oxide, 4-hydroxypyridine, LH-20 sephadex gel, 4,4′-dimethyl-2,2′-bipyridine, butyllithium solution (1.6 M in hexane), 2-ethylhexyl iodide were purchased from Aldrich. Diisopropylamine was obtained from Merck. 4-(5-nonyl) pyridine (dnpy) was provided from ABCR. All reactions and manipulations of air-sensitive materials were carried out under argon atmosphere and using standard Schlenk techniques. Solvents were dried and freshly distilled prior to use. All other chemicals were used as received.

2.1.2. Materials for the fabrication of DSSCs

Commercially available lithium iodide, iodine, 1-methyl-3-propylimidazolium iodide, tert-butyl pyridine, guanidine thiocyanate, hydrogen hexachloroplatinate(IV) hydrate (H_2PtCl_6), poly(propylene glycol) bis(2-aminopropyl) ether, 3-isocyanatopropyltriethoxysilane and all solvents were purchased from Sigma-Aldrich. SnO_2:F transparent conductive electrodes (FTO, TEC^{TM} A8) 8 Ohm/square were purchased from Pilkington NSG Group. Commercial ultra pure titanium isopropoxide (TTIP, 97%, Aldrich), Triton X-100 (polyoxyethylene-10-isooctylphenyl ether) surfactant (99.8%, Aldrich), glacial acetic acid (AcOH, Aldrich) were used to make TiO_2 precursor sols. Titania powder P25 was provided by Degussa, (Germany, 30% Rutile and 70% Anatase).

2.2. Preparation of TiO_2 photoelectrodes

TiO_2 films were fabricated in two steps. A thin layer of TiO_2 was first deposited on FTO glass substrates as blocking layer via sol-gel method following a previously reported procedure [23,24]. Briefly, for 5.4 ml solution, 0.72 g of Triton X-100 was mixed with 4 ml of ethanol, followed by addition of 0.4 ml of glacial acetic acid and 0.32 ml of titanium isopropoxide under vigorous stirring. After a few minutes stirring, FTO glasses were dipped in the above sol and withdrawn with 2 cm/sec. The films were heated up to 500 °C for 30 minutes using 20 °C/min heating ramp rate. The procedure was applied for the deposition of only one TiO_2 layer while the film thickness was approximately 150 nm. Then, a second thicker layer was coated on top of the above layer, made of nanocomposite TiO_2 paste using P25 commercial powder by doctor blade technique, followed by heating to 500 °C. The fabrication of TiO_2 paste was as follows: 3 g of Degussa P25 was mixed with 0.5 ml of acetic acid in a mortar for about 3 min. After that, 2.5 ml of millipore water and 17.5 ml of ethanol were alternately added to break all TiO_2 aggregates and form a homogenous solution. The solution was transferred to a crucible with 50 ml of ethanol and was mixed with 10 g of terpineol and an amount of ethyl cellulose. The solution was ultrasonicated for about 2 minutes and then the crucible was placed in a rotary evaporator at 40–45 °C to remove the excessive solvent and form the TiO_2 paste.

2.3. Preparation of Ligands and Ruthenium Complexes

The ligands 4,4′-dicarboxy-2,2′-bipyridine (L_1), 4,4′-bis(3-ethylheptyl)-2,2′-bipyridine (L_2), 4-(3-ethylheptyl)-4′-methyl 2,2′-bipyridine (L_3), 4-heptyl-4′-methyl-2,2′-bipyridine (L_4), 4-dihexylmetyl-4′-heptyl-2,2′-bipyridine (L_5), 4-(2-ethyl-hexyloxy)-pyridine (L_6) and their heteroleptic ruthenium(II) complexes of the type $[RuL_1L_2(NCS)_2]$ (CS27), $[RuL_1L_3(NCS)_2]$ (CS28), $[RuL_1L_4(NCS)_2]$ (CS32), $[RuL_1L_5(NCS)_2]$ (CS43), $[RuL_1L_6(NCS)_3]$ (CS17), $[RuL_1(dnpy)(NCS)_3]$ (CS22) was prepared and purified according to the procedure reported in literature [25]. The molecular structures of the six ruthenium complexes are given in Scheme 1.

2.4. Fabrication and characterization of quasi-solid state dye-sensitized solar cell

2.4.1. Dye-sensitization of TiO_2 films

The new dye solutions were prepared using N,N dimethylformamide (DMF) as a solvent. To compare the new dye complexes with a commercially available dye we used D907 purchased from Everlight Co. with similar chemical structure (Scheme 1). All TiO_2 films were immersed in the ruthenium dye solutions (1 mM) overnight in order to complete the photoanode preparation. Thus, some TiO_2 films where sensitized using a 1 mM acetonitrile solution of D907.

2.4.2. Quasi-solid electrolyte preparation

In the construction of the solar cells a quasi-solid state electrolyte was used. This was chosen as a promising technique to DSSC technology as it combines the high ionic conductivity of liquids while it reduces the risk of leaks and minimizes sealing problems in the cells. For the gel electrolyte applied to the DSSCs, we used a hybrid organic-inorganic material which was prepared according to a procedure described in previous publications [26,27]. Briefly, poly(propylene glycol) bis(2-aminopropyl ether) of molecular weight 230 and 3-isocyanatopropyltriethoxysilane (ICS; molar ratio ICS/diamine = 2) react in a vessel (acylation reaction), producing urea connecting groups between the polymer units and the inorganic part. The gel electrolyte was synthesized by

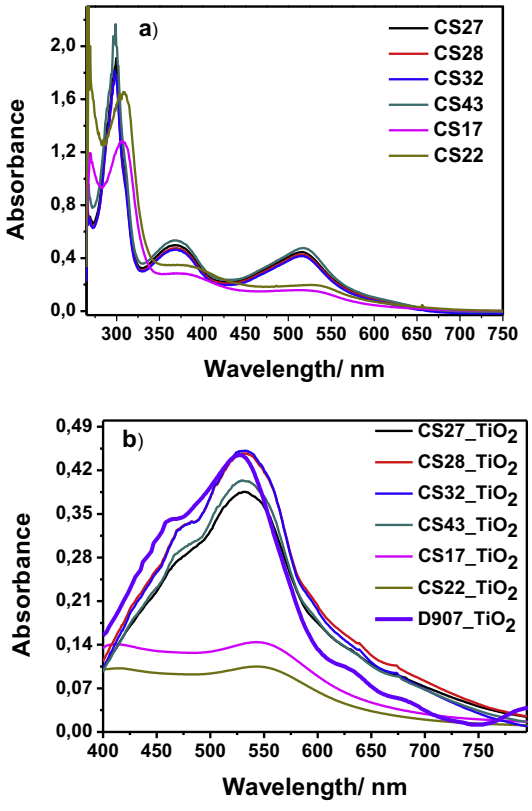

Fig. 1. (a) UV–vis absorption spectra of 4×10^{-5} M solution of bpy-bpy ruthenium complexes (CS27, CS28, CS32, CS48) and bpy-py ruthenium complexes (CS17, CS22) in DMF, (b) UV–vis absorption spectra of ruthenium dyes adsorbed on TiO_2 film.

Table 1
Absorption and electrochemical data of the ruthenium complexes in DMF.

Complex	λ_{max}, (nm) ($e/10^4 M^{-1}.cm^{-1}$)					
	$\pi \rightarrow \pi^*$	d $\pi \rightarrow \pi^*$	E_{ox} (V) (ΔE_p (V))	E_{red1}(V)	E_{red2} (V) (ΔE_p (V))	E_{red3} (V) (ΔE_p (V))
CS27	299 (4.78)	369 (1.25) 517 (1.13)	0.96 (0.010)	-1.12	-1.46 (0.056)	-1.77 (0.013)
CS28	299 (4.48)	370 (1.20) 518 (1.08)	0.99 (0.009)	-1.09	-1.45 (0.065)	-1.76 (0.021)
CS32	298 (4.50)	370 (1.17) 518 (1.05)	0.97 (0.008)	-1.1	-1.42 (0.009)	-1.76 (0.017)
CS43	299 (5.43)	369 (1.34) 518 (1.20)	0.99 (0.010)	-1.11	-1.43 (0.009)	-1.77 (0.017)
CS17	306 (3.23)	382 (0.71) 530 (0.41)	1.25 (0.096)	-0.73	-1.34	-1.61
CS22	305 (2.60)	386 (0.85) 533 (0.50)	1.25 (0.104)	-0.71	-1.33	-1.57

the following procedure: 0.7 grams of the functionalized alkoxide precursor were dissolved in 1.6 grams of sulfolane and 0.8 grams of 3-methoxypropionitrile under vigorous stirring. Then, 0.368 g AcOH were added followed by 0.3 M 1-methyl-3-propylimidazolium iodide, 0.1 M LiI and 0.05 M I_2 in a final molar ratio AcOH:LiI:MPImI:I_2 = 2.5:0.1:0.3:0.05. To complete the electrolyte solution, 0.204 g of tert-butyl pyridine and 0.036 g of guanidine thiocyanate were added to the above mixture. After six hours stirring, one drop of the obtained sol was placed on the top of the titania electrode with adsorbed dye molecules and a slightly platinized FTO counter electrode was pushed by hand on the top. The platinized FTO glass was made by casting a few drops of H_2PtCl_6 solution (5 mg/1 ml of ethanol) followed by heating at 500 °C for 10 minutes. The two electrodes tightly stuck together by Si-O-Si bonds developed by the presence of the hybrid material.

2.5. Characterization techniques

UV-Vis spectra were recorded in a 1 cm path length quartz cell by using Analytic Jena S 600 UV spectrophotometer. Infrared spectra were obtained with a Perkin Elmer, Spectrum BX-FTIR spectrophotometer. NMR spectra were recorded at 297 K on a Varian Mercury AS 400 NMR instrument at 400 MHz (^{1}H) and 100.56 MHz (^{13}C). Electrochemical data were obtained using a CH Instrument 660 B Model Electrochemical Workstation. Cyclic voltammograms were measured in a cell containing a glassy carbon working electrode, silver wire reference electrode, platinum wire counter electrode and supporting electrolyte consisting of 0.1 M $TBAPF_6$ in DMF with a scan rate of 100 mVs^{-1}. The ferrocenium/ferrocene couple was used as an internal standard (0.65 V *vs.* Ag/Ag^+).

For the *J-V* curves, the samples were illuminated with Xe light using a Solar Light Co. solar simulator (model 16S-300) equipped with AM 0 and AM 1.5 direct Air Mass filters to simulate solar radiation at the surface of the earth. The light intensity was kept constant at 1000 W/m^2 measured with a CMP 3 Kipp & Zonen pyranometer. Finally, the *J-V* curves were recorded by connecting the cells to a Keithley Source Meter (model 2601 A) which was controlled by Keithley computer software (LabTracer). The cell active area was constant to 0.3 cm^2 using appropriate mask while back reflectors were not used in the measurements. For each case, we made two devices which were tested under the same conditions in order to avoid any misleading estimation of their efficiency. Cell performance parameters, including short-circuit current density (J_{SC}), open circuit voltage (V_{OC}), maximum power (P_{max}), fill factor (*FF*) and overall cell conversion efficiency, were measured and calculated from each *J-V* characteristic curve. Besides, incident photon-to-current efficiency (IPCE) was measured for all cells after illumination with Xe light source using a filter monochromator (IQE 200^{TM}, Newport).

Impedance measurements were carried out under illumination using the same Xe light source that was used for the *J-V* curves. EIS measurements were performed without the use of a mask with Metrohm Autolab 3.v potentiostat galvanostat (Model PGSTAT 128 N) through a frequency range of 100 kHz–0.01 Hz using a perturbation of ±10 mV over the open circuit potential. Experimental data are presented by scattering symbols while lines represent the fitted plots obtained using Nova 1.10 software.

3. Results and Discussion

3.1. Absorption studies

The absorption spectra of the ruthenium complexes in DMF are shown in Fig. 1a and maximum absorption wavelengths and the molar absorption coefficients are summarized in Table 1. The absorption spectra of ruthenium complexes show bands between 370 and 533 nm that are assigned to metal-to-ligand charge transfer (MLCT) transitions. In the UV region, the bands below 306 nm are observed due to the π-π^* transitions of bipyridine and

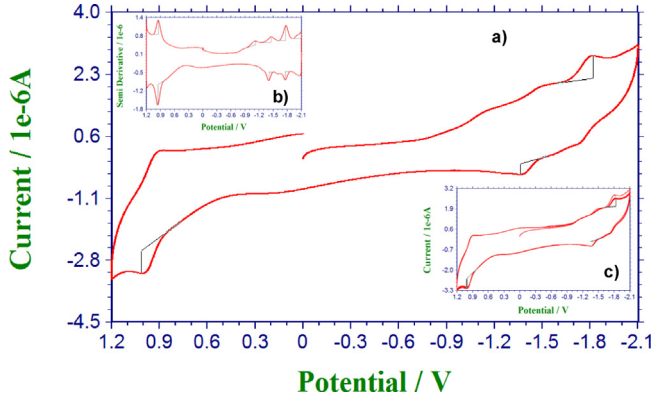

Fig. 2. (a) Cyclic voltammograms of CS27, (b) differential of CS27 voltammogram, (c) 5 consecutive cyclic voltammograms of CS27 measured in DMF solutions with scan speed of 100 mVs^{-1}.

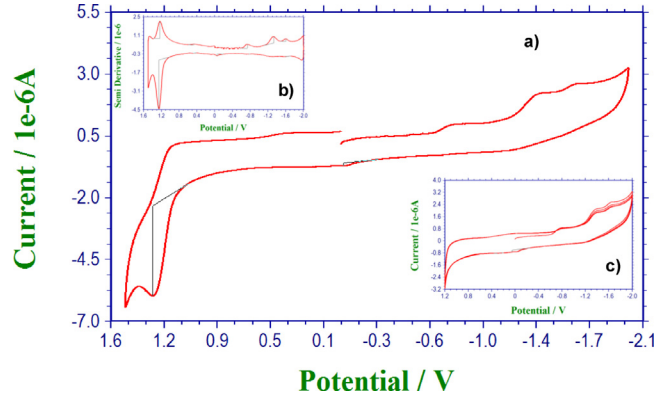

Fig. 3. (a) Cyclic voltammograms of CS17, (b) differential of CS17 voltammogram, (c) 5 consecutive cyclic voltammograms of CS17 measured in DMF solutions with scan speed of 100 mVs^{-1}.

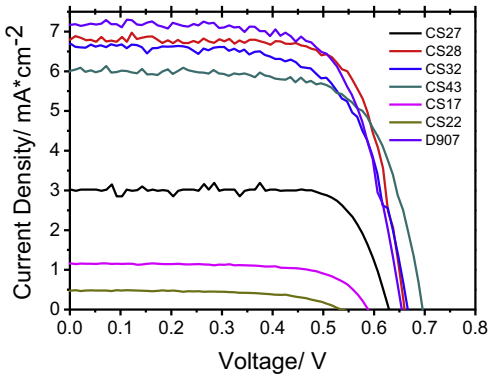

Fig. 4. Photocurrent-voltage curves of DSSCs with TiO_2 nanocrystalline films sensitized with different newly fabricated ruthenium dyes.

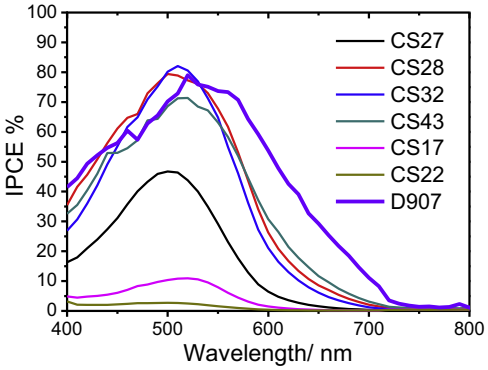

Fig. 5. Dark current-voltage characteristic curves of dye-sensitized solar cells with different dyes.

pyridine ligands [28,29]. The bpy-bpy molecules containing branching and non-branching side groups (CS27, CS28, CS32, CS43) exhibit similar maximum absorption wavelengths and the molar absorption coefficients (Fig. 1a). This indicates that branching of side groups was not important effect on absorption properties [28]. The absorption spectra of bpy-py molecules (Fig. 1a) show blue shifted the lowest-energy MLCT band from 533 nm to 530 nm in the bpy-py molecule with –C–O–C–molecular group in the side group (CS17). The blue shift is attributed to the donor character of 4-(2-ethyl-hexyloxy)-pyridine ligands containing oxygen in side group which cause in a slight increase in energy of the LUMO of the complex [30]. This results that the π-π^* and MLCT transitions occur at higher energy.

In comparison to bpy-bpy molecules (CS27, CS28, CS32, CS43), the lowest-energy MLCT band of bpy-py molecules (CS17, CS22) is red shifted by 12 nm while the molar extinction coefficient decreases. The red shift is due to the fact that the pyridine rings in bpy-py molecules may rotate free into the optimum overlap configuration [31]. The more conjugated character of bpy-bpy molecules result an increase in the molar extinction coefficient. It is very important to develop sensitizers with high molar extinction coefficients which increase solar light harvesting capacity [32]. Improving the molar extinction coefficients of sensitizers can result in an increasing efficiency in DSSC applications. The bpy-bpy molecules (ε: 1.05-1.34 $\times 10^4\,M^{-1}\cdot cm^{-1}$) exhibit similar molar extinction coefficients compared to one of the standard dyes, D907 in literature (ε: $1.16 \times 10^4\,M^{-1}\cdot cm^{-1}$) [28].

In order to obtain concrete results about the amount of dye on TiO_2 films which could be correlated with electrical characterization results, we performed UV–vis absorption measurements to examine the light absorption spectra of the dyes on TiO_2 films (Fig. 1b). It is obvious that the absorbance of the two complexes CS28 and CS32 is directly compared with that obtained for D907 while the absorbance of the other two bpy-bpy molecules CS43 and CS27 is a little less. In accordance to the Fig. 1a the absorbance of the two bpy-py molecules CS17 and CS22 is much lower while the optical impression of the films is that they possess a very pale purple color which finally affected to the overall performance of the cells as it can be seen to the next paragraphs.

Table 2
Solar cells parameters for DSSCs with TiO_2 photoelectrodes sensitized with different ruthenium dyes.

Complex	J_{SC} (mA/cm^2)	V_{oc} (Volts)	*FF*	n (%)
CS27	3.0	0.63	0.77	1.46
CS28	7.0	0.66	0.72	3.28
CS32	6.7	0.66	0.67	2.95
CS43	6.1	0.69	0.69	2.91
CS17	1.2	0.59	0.69	0.47
CS22	0.5	0.53	0.62	0.16
D907	7.3	0.65	0.69	3.26

3.2. Electrochemical Data

Electrochemical properties of the complexes have been investigated by cyclic voltammetry. The electrochemical data are summarized in Table 1 and the cyclic voltammograms of CS27 and CS17 are given in Fig. 2 and 3. The cyclic voltammogram of the bpy-bpy molecules (CS27, CS28, CS32, CS43) show one reversible oxidation peak around 0.97 V vs. Ag/Ag^+, which is attributed to the Ru (II/III) couple (Fig. 2a). The quasi-reversible oxidation peaks of bpy-py (CS17, CS22) (Fig. 3a) show anodic shift from 0.97 V to 1.25 V compared to bpy-bpy molecules (CS27, CS28, CS32, CS43). This means that electron density of ruthenium metal for bpy-py is less than that for bpy-bpy complexes [25]. This is attributed to chelating effect of bidentate bipyridine ligands. The chelating effect increases the interaction between ruthenium and bipyridyl nitrogens (Ru–N), the greater the π-back bonding, which leads to a shorter Ru–N bond length compared to monodentate coordination [25]. This interaction occur by the electron donation from bipyridine ligand to empty ruthenium metal d orbital and followed by the π-back bonding from the filled ruthenium metal d orbital to the empty π^* orbital of ligand. This interaction increase electron density in the ruthenium metal t_{2g} orbital in the presence of bipyridine ligand which coordinates to ruthenium metal with two electron donating nitrogens [33–35]. This result in a cathodic shift for bpy-bpy molecules compared to bpy-py molecules. The cyclic

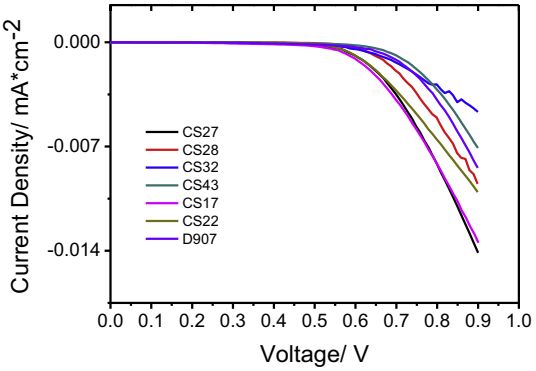

Fig. 6. (a) Impedance spectra and (b) Bode phase plots of dye-sensitized solar cells with different dye complexes measured at open circuit voltage at 1 sun illumination.

voltammograms of the bpy-bpy and bpy-py molecules (Fig. 2b and 3b) show three reduction peaks. The reduction peaks are assigned to the reduction of carboxylic acid protons, 4,4′-dicarboxy- 2,2′-bipyridine and the bipyridine, respectively [28]. The reduction potentials of bpy-bpy molecules are shifted cathodically which are related to the stronger electron donor property of bipyridine ligands.

Consecutive cyclic behaviors of the complexes (Fig. 2c and 3c) were investigated in order to determine their electrochemical stability. The bpy-bpy molecules have more electrochemical stability compared to the bpy-py molecules. No significant change in peak currents and potentials of anodic and cathodic areas are observed in bpy-bpy molecules. Furthermore, the reversibility of the redox peaks exhibits more stability of bpy-bpy molecules. It indicates that the chelating effect enhances stability in the presence of bipyridine ligand [25].

The energy levels and electrochemical stability of the complexes are in agreement with the reported values for the related classes of ruthenium(II) complexes and can be used as photosensitizers in DSSCs [28–30].

3.3. Solar cells performance

The current-voltage (*J-V*) characteristic curves of quasi solid-state dye sensitized solar cells, for all the dye complexes tested are presented in Fig. 4. In all *J-V* measurements, a mask with an aperture area of 0.3 cm^2 was used. In general, cells sensitized with the new dye complexes showed almost the same overall performance compared with the ones that were sensitized with D907. In the case of CS28 a slight better performance was monitored than this obtained for D907. Some of the new dyes weren't adsorbed that well (Fig. 1(b)), so they didn't sensitize sufficiently the TiO_2 films which was reflected to the obtained current density values.

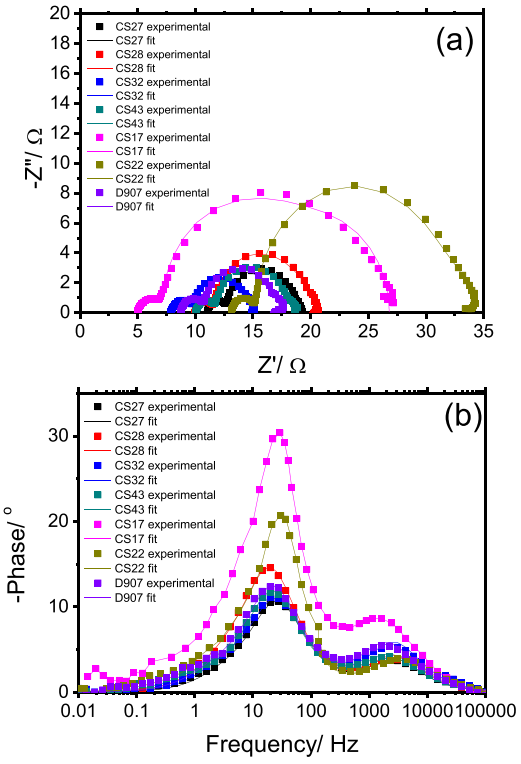

Fig. 7. DSSCs equivalent circuits (a) R(RC)(RC)(RC) and (b) R(RQ)(RQ)(RQ) used to fit the experimental data from the EIS measurements.

The electrical parameters measured and calculated for all cells are summarized in Table 2. The bpy-bpy molecules (CS32, CS28, CS43) showed higher cell efficiency in the range of 2.9%-3.3% compared to the bpy-py molecules (CS17, CS22). The more conjugated character of bpy-bpy molecules result in an increase in the molar extinction coefficients. This can enhance solar light harvesting capacity and improve the conversion efficiencies of DSSCs [36]. It is worth noting that the cells sensitized with the dyes CS28, CS32 and CS43 showed a slightly increased open circuit voltage compared with D907. The cell efficiency of CS27 decreased in the presence of two branching alkyl chains when compared to other bpy-bpy molecules. This increase in efficiency of cells can be attributed to decreasing steric effect of side groups. The cell efficiency of CS17 is higher than CS22 which may be attributed to more electron donor properties of pyridine ligand containing oxygen in side group of CS17. The performance of the new dyes as TiO_2 sensitizers in DSSCs was also explained in terms of the external quantum efficiency measured for each cell employing the six ruthenium complexes. Fig. 5 presents the IPCE values of the dyes at different wavelengths. It can be seen that the maximum of the cell efficiency almost coincides with the maximum of the dye absorption spectra of the dyes on TiO_2. It can also be seen that the better *Jsc* values obtained for D907 can be attributed to the extension of the IPCE spectrum at longer wavelengths compared to that obtained for CS28 and CS32. However, values exceeding 80% are obtained for these dyes (CS28, CS32) while 70% and 45% IPCE values are monitored for the rest two bpy-bpy molecules CS43 and CS27 respectively. Finally, low IPCE values for the two bpy-py molecules are obtained which are in line with *J-V* data.

The cells with the different ruthenium dyes were also examined as efficient photoelectrodes in DSSCs measuring the dark current suppression. Fig. 6 shows that dark current density in the cells made with the new dyes does not have substantial differences compared to that obtained for D907 dye. However, the electron leakage, in the cells made with the dyes CS17 and CS22 is noticeably higher compared to the cells with the dyes CS28, CS32, CS43 and D907 which can be attributed the poor adsorption of these dyes in the TiO_2 mesoporous films and it finally leads to a reduced overall performance under light exposure.

3.4. Electrochemical Impedance Spectroscopy (EIS)

Fig. 7a and b show the Nyquist and Bode plots obtained from cells with the different ruthenium dyes respectively. The first semicircle, starting from left to right, corresponds to the Pt/electrolyte interface, R_{pt}. The charge transfer resistance at the counter electrode (R_{pt}) is represented as a semicircle in the impedance spectra and a peak in the Bode phase angle plot (peak at high frequency). The resistance element related to the response in the intermediate frequency represents the charge transport at the

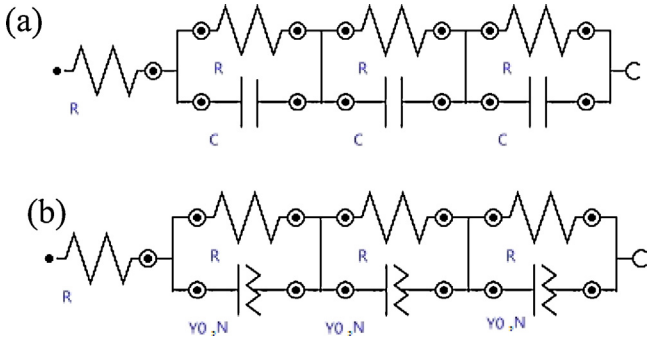

Fig. 8. DSSCs equivalent circuits (a) R(RC)(RC)(RC) and (b) R(RQ)(RQ)(RQ) used to fit the experimental data from the EIS measurements.

Table 3
Fitted parameters derived from electrochemical impedance spectroscopy.

Complex	R_h (Ω)	R_{pt} (Ω)	C_{pt} (F) (10^{-4})	R_{tr} (Ω)	C_{tr} (F) (10^{-3})	R_{dif} (Ω)	C_{dif} (F) (10^{-1})
CS27	11.10	1.59	0.42	5.60	1.31	0.81	0.65
CS28	10.00	1.56	0.40	7.37	1.40	1.48	0.39
CS32	7.96	1.75	0.38	4.40	1.72	1.00	0.55
CS43	10.10	1.63	0.46	6.00	1.50	0.99	1.56
CS17	5.07	2.00	0.65	11.7	1.63	8.02	0.12
CS22	13.20	2.02	0.35	16.40	1.64	2.58	0.93
D907	8.78	1.91	0.45	5.70	1.58	1.03	0.75

TiO_2/dye/electrolyte interface (R_{tr}) and shows diode like behavior. The charge transfer resistance (R_{pt}) must not be confused with the electron or charge transport resistance (R_{tr}) as these terms are used to describe the real part of two different impedances which are represented by two different semicircles [37]. The semicircle at the low frequency, which is attributed to the diffusion of redox species in the electrolyte (R_{dif}), was small and not well formed indicating a fast diffusion. Finally, the intercept of the horizontal axis stands for the resistance of the sheet resistance of the FTO substrate and the contact resistance of the FTO/TiO_2 (R_h) [38,39].

The total series resistance of the cell can be calculated using Eq. (1):

$$R_S = R_h + R_{pt} + R_{dif} \quad (1)$$

The semicircles at the Nyquist plots are obtained from a frequency scan through a wide range of high, intermediate and low frequency [40]. Thus, the Bode phase plots also features three characteristic frequency peaks corresponding to each of the Nyquist characteristic peaks.

The equivalent circuits which were used to fit the experimental data are presented in Fig. 8. For electrodes having a rough surface the capacitance element in Fig. 8 is replaced by a constant phase element (CPE, Q) which depends on the parameters Y_o and N [41]. According to instrument software's manual Y_o is the admittance of an ideal capacitance while N is an empirical constant ranging from 0 to 1. It is possible to convert a CPE element, which is in parallel with a resistance, to a pseudo capacitance using Eq. (2).

$$C_{pseudo} = Y_O^{1/N} \cdot R^{\left(\frac{1}{N}-1\right)} \quad (2)$$

As shown from Eq. (2) for N = 1 the CPE element describes a pure capacitor while for N = 0 an ideal resistor. Moreover for N = 0.5 the CPE element is equivalent to the Warburg element often used to describe the diffusion in the electrolyte. It is generally though to arise from the lack of homogeneities in the electrode–material system. The fitted parameters are presented in Table 3. The values of R_{pt}, C_{pt}, R_{dif} and C_{dif} were almost invariable as all cells were fabricated using the same electrolyte solution and the same type of counter electrode. The main variation was observed in R_{tr} and C_{tr} values. Cells with less dye adsorbed, exhibit an increased charge transport resistance at the TiO_2/dye/electrolyte interface. A small R_{tr} value with a simultaneous high C_{tr} value denotes a fast charge transport at the interface of TiO_2/dye/electrolyte, which explains the better overall performance of the cells sensitized with the dyes CS32, CS28, CS43 and D907 [42].

The electron lifetime τ_n, in DSSC is of great importance to determine the recombination dynamics in the cell. The electron lifetime of all the cells was calculated using Eq. (3), where f is the mid-frequency peak from the Bode phase plots.

$$\tau_n = \frac{1}{2 \cdot \pi \cdot f} \quad (3)$$

The electron lifetime for the cells with CS28 was slightly higher than the ones with D907. Particularly, as shown in Table 4, the electron lifetime was 8.10 and 8.08 ms for the cells with CS28 and D907 respectively which sounds as an improvement to the cells employing newly synthesized CS28 dye.

Table 4
Electron lifetime derived from electrochemical impedance spectroscopy

Complex	f (Hz)	τ_n (ms)
CS27	27.00	5.89
CS28	19.66	8.10
CS32	26.91	5.91
CS43	19.11	8.07
CS17	29.38	5.42
CS22	30.33	5.25
D907	19.69	8.08

Table 5
Electron diffusion length derived from electrochemical impedance spectroscopy.

Complex	$\frac{R_{tr}}{R_{dif}}$	L_n (μm)
CS27	6.91	13.15
CS28	4.98	11.16
CS32	4.00	10.49
CS43	6.06	12.31
CS17	1.46	6.04
CS22	6.36	12.61
D907	5.53	11.76

Electron collection efficiency is vitally important to determine the photovoltaic performance of a DSSC. Electron collection in the conducting substrate can be described in terms of electron diffusion length, L_n. Using the electrochemical parameters from the impedance results and the thickness of TiO_2 film, L_n can be calculated from the expression: $L_n = L \cdot \sqrt{\frac{R_{tr}}{R_{dif}}}$, where L is the film thickness of the TiO_2 [43]. For a relatively ~5 micrometers thick TiO_2 layer the data for all aforementioned solar cells employing the new dyes are presented in Table 5. It is worth noting that most of the cells made with the new dyes showed quite comparable results with the cell employing commercial dye D907. The L_n values were calculated in the range of 10–13 micrometers.

4. Conclusion

In this work, we reported the effect of pyridine and bipyridine with different side groups in ruthenium dye complexes on absorption and electrochemical properties. The obtained results showed the branching of side groups was not important effect on absorption and electrochemical properties. However, the more conjugated character of bpy-bpy molecules resulted in an increase in the molar extinction coefficient which improved cell efficiency in DSSC applications compared to bpy-py molecules.

The performance of the ruthenium complexes as photosensitizer in quasi solid-state dye sensitized solar cells was studied under the same conditions and bpy-bpy molecules showed almost the same overall cell performance compared with D907. The cell performance of CS28 was finally a slight better than D907 exhibiting an overall conversion efficiency of 3.28% compared to 3.26% of the commercial D907. However, a decrease in cell performance was observed in the presence of pyridine for CS17 and CS22 which was attributed to the poor adsorption of these dyes in the TiO_2 mesoporous films and lower values for extinction coefficients. The EIS characterization of the aforementioned cells with the six dyes showed lower values for local resistance to charge transfer across the TiO_2-electrolyte interface for CS28 and CS32 bipyridine complexes (1.55/1.75 ohms respectively) compared to D907 (1.91 ohms). Furthermore, quite comparable values for free electron lifetimes and electron diffusion lengths for most of the cells employing new dyes and commercial D907 were monitored.

Acknowledgement

D. Sygkridou and E. Stathatos acknowledge that their research has been co-financed by the European Union (European Social Fund - ESF) and Greek national funds through the Operational Program "Education and Lifelong Learning" of the National Strategic Reference Framework (NSRF) - Research Funding Program: ARCHIMEDES III, Investing in knowledge society through the European Social Fund.

References

[1] B. O'Regan, M. Grätzel, A low-cost, high-efficiency solar cell based on dye-sensitized colloidal TiO_2 films, Nature 353 (1991) 737–740.
[2] A. Hagfeldt, G. Boschloo, L. Sun, L. Kloo, H. Pettersson, Dye-Sensitized Solar Cells, Chemical Reviews 110 (2010) 6595–6663.
[3] J.-H. Yum, P. Chen, M. Grätzel, M.K. Nazeeruddin, Recent Developments in Solid-State Dye-Sensitized Solar Cells, ChemSusChem 8-9 (2008) 699–707.
[4] Md. K. Nazeeruddin, E. Baranoff, M. Gräetzel, Dye-sensitized solar cells: A brief overview, Solar Energy 85 (2011) 1172–1178.
[5] J. Durrant, S.A. Haque, E. Palomares, Photochemical energy conversion: from molecular dyads to solar cells, Chem. Commun. 31 (2006) 3279–3289.
[6] K. Kakiage, Y. Aoyama, T. Yano, T. Otsuka, T. Kyomen, M. Unno, M. Hanaya, An achievement of over 12 percent efficiency in an organic dye-sensitized solar cell, Chem. Commun. 50 (2014) 6379–6381.
[7] X. Pan, M. Wang, X. Fang, C. Zhang, Z. Huo, S. Dai, Ionic liquid crystal-based electrolyte with enhanced charge transport for dye-sensitized solar cells, Science China Chemistry 56 (2013) 1463–1469.
[8] B.O' Regan, J. Durrant, Kinetic and energetic paradigms for dye sensitized solar cells: Moving from the ideal to the real, Accounts of Chemical Research 42 (2009) 1799–1808.
[9] M. Grätzel, In Nanostructured materials for Electrochemical Energy Production and Storage, in: E.R. Leite (Ed.), Springer-Verlag, New York, 2008.
[10] J.-H. Yum, I. Jung, C. Baik, J. Ko, M.K. Nazeeruddinand, Michael Grätzel, High efficient donor–acceptor ruthenium complex for dye-sensitized solar cell applications, Energy Environ. Sci. 2 (2009) 100–102.
[11] M.-E. Ragoussi, M. Ince, T. Torres, Recent Advances in Phthalocyanine-Based Sensitizers for Dye-Sensitized Solar Cells, Eur. J. Org. Chem. 29 (2013) 6475–6489.
[12] T. Moehl, H.N. Tsao, K.-L. Wu, H.-C. Hsu, Y. Chi, E. Ronca, F. De Angelis, M.K. Nazeeruddin, M. Grätzel, High Open-Circuit Voltages: Evidence for a Sensitizer-Induced TiO_2 Conduction Band Shift in Ru(II)-Dye Sensitized Solar Cells, Chem. Mater. 25 (22) (2013) 4497–4502.
[13] A. Mishra, M.K.R. Fischer, Peter Bauerle, Metal-Free Organic Dyes for Dye-Sensitized Solar Cells: From Structure: Property Relationships to Design Rules, Angew. Chem. Int. Ed. 48 (2009) 2474–2499.
[14] K.-L. Wu, S.-T. Ho, C.-C. Chou, Y.-C. Chang, H.-A. Pan, Y. Chi, P.-T. Chou, Engineering of Osmium(II)-Based Light Absorbers for Dye-Sensitized Solar Cells, Angewandte Chemie International Edition 23 (2012) 5642–5646.
[15] J. Jin, Y. Shan, F. Yang, H. Lai, H. Tan, X. Liu, J. Tang, Q. Fang, Organic photosensitizers with N-carboxymethyl pyridinium acceptor/anchoring group for dye-sensitized solar cells, Synthetic Metals 162 (2012) 2222–2227.
[16] L. Wang, X. Yang, S. Li, M. Cheng, L. Sun, A new type of organic sensitizers with pyridine-N-oxide as the anchoring group for dye-sensitized solar cells, RSC Adv 3 (2013) 13677–13680.
[17] H. Zhou, L. Wu, Y. Gao, T. Ma, Dye-sensitized solar cells using 20 natural dyes as sensitizers, Journal of Photochemistry and Photobiology A: Chemistry 219 (2011) 188–194.
[18] P. Qin, X. Yang, R. Chen, L. Sun, Influence of π-Conjugation Units in Organic Dyes for Dye-Sensitized Solar Cells, J. Phys. Chem. C 111 (2007) 1853–1860.
[19] M. Zalas, B. Gierczyk, M. Klein, K. Siuzdak, T. Pędziński, T. Łuczak, Synthesis of a novel dinuclear ruthenium polypyridine dye for dye-sensitized solar cells application, Polyhedron 67 (2014) 381–387.
[20] L. Han, A. Islam, H. Chen, C. Malapaka, B. Chiranjeevi, S. Zhang, X. Yang, M. Yanagida, High-efficiency dye-sensitized solar cell with a novel co-adsorbent, Energy Environ. Sci. 5 (2012) 6057–6060.
[21] C.-Y. Li, C. Su, H.-H. Wang, P. Kumaresan, C.-H. Hsu, I.-T. Lee, W.-C. Chang, Y.S. Tingare, T.-Y. Li, C.-F. Lin, W.-R. Li, Design and development of cyclometalated ruthenium complexes containing thiophenyl-pyridine ligand for dye-sensitized solar cells, Dyes and Pigments 100 (2014) 57–65.
[22] H. Ozawa, S. Honda, D. Katano, T. Sugiura, H. Arakawa, Novel ruthenium sensitizers with a dianionic tridentate ligand for dye-sensitized solar cells: the relationship between the solar cell performances and the electron-withdrawing ability of substituents on the ligand, Dalton Trans. 43 (2014) 8026–8036.
[23] E. Stathatos, P. Lianos, C. Tsakiroglou, Highly efficient nanocrystalline titania films made from organic/inorganic nanocomposite gels, Microporous and Mesoporous Materials 75 (2004) 255–260.
[24] T. Makris, V. Dracopoulos, T. Stergiopoulos, P. Lianos, A quasi solid-state dye-sensitized solar cell made of polypyrrole counter electrodes, Electrochimica Acta 56 (2011) 2004–2008.
[25] C. Sahin, C. Th Dittrich, Varlikli, S. Icli, M.C. Lux-Steiner, Role of side groups in pyridine and bipyridine ruthenium dye complexes for modulated surface photovoltage in nanoporous TiO_2, Solar Energy Materials and Solar Cells 94 (2010) 686–690.
[26] E. Stathatos, Organic-inorganic nanocomposite materials prepared by the sol-gel route as new ionic conductors in quasi solid state electrolytes, Ionics 11 (2005) 140–145.
[27] E. Stathatos, P. Lianos, U.L. Stangar, B. Orel, P. Judeinstein, Structural Study of Hybrid Organic/Inorganic Polymer Gels Using Time-Resolved Fluorescence Probing, Langmuir 16 (2000) 8672–8676.
[28] Md. K. Nazeeruddin, S.M. Zakeeruddin, J.-J. Lagref, P. Liska, P. Comte, C. Barolo, G. Viscardi, K. Schenk, M. Graetzel, Stepwise assembly of amphiphilic ruthenium sensitizers and their applications in dye-sensitized solar cell, Coordination Chemistry Reviews 248 (2004) 1317–1328.
[29] C. Sahin, C. Varlikli, C. Zafer, Q. Shi, R.E. Douthwaite, A new 1H-pyridin-(2E)-ylidene ruthenium complex as sensitizer for a dye-sensitized solar cell, Journal of Coordination Chemistry 66 (8) (2013) 1384–1395.
[30] C. Klein, M.K. Nazeeruddin, D.D. Censo, P. Liska, M. Grätzel, Amphiphilic ruthenium sensitizers and their applications in dye-sensitized solar cells, Inorganic Chemistry 43 (2004) 4216–4226.
[31] M. Haga, E. Dodsworth, A.B.P. Lever, Catechol-quinone redox series involving bis(bipyridine) ruthenium(II) and tetrakis(pyridine) ruthenium(II), Inorg. Chem. 25 (1986) 447–453.
[32] D. Kuang, S. Ito, B. Wenger, C. Klein, J.E. Moser, R. Humphry-Baker, S.M. Zakeeruddin, M. Graetzel, High Molar Extinction Coefficient Heteroleptic Ruthenium Complexes for Thin Film Dye-Sensitized Solar Cells, J. Am. Chem. Soc. 128 (2003) 4146–4154.
[33] T.J.J. Kinnunen, M. Haukka, E. Pesonen, T.A. Pakkanen, Ruthenium complexes with 2,20-2,40 and 4,40-bipyridine ligands: the role of bipyridine coordination modes and halide ligands, J. Organomet. Chem. 655 (2002) 31–38.
[34] T.J.J. Kinnunen, M. Haukka, T.A. Pakkanen, Alkoxycarbonyl substituted ruthenium mono(bipyridine) complexes: steric effects of the bipyridine substituents, J. Organomet. Chem. 654 (2002) 8–15.
[35] F.M. Weller, T. Overton, J. Rourke, F. Armstrong, Inorganic Chemistry, Oxford University Press, United Kingdom, 2014.
[36] B.P. Wang, S.M. Zakeeruddin, J.E. Moser, R. Humphry-Baker, P. Comte, V. Aranyos, A. Hagfeldt, Md K. Nazeeruddin, M. Gratzel, Stable New Sensitizer with Improved Light Harvesting for Nanocrystalline Dye-Sensitized Solar Cells, Adv. Mater. 16 (2004) 1806–1811.
[37] R. Guliani, A. Jain, A. Kapoor, Exact analytical analysis of dye-sensitized solar cell: improved method and comparative study, The Open Renewable Energy Journal 5 (2012) 49–60.
[38] F. Fabregat-Santiago, G. Garcia-Belmonte, I. Mora-Seró, J. Bisquert, Characterization of nanostructured hybrid and organic solar cells by impedance spectroscopy, Phys. Chem. Chem. Phys. 13 (2011) 9083–9118.
[39] Q. Wang, J.-E. Moser, M. Grätzel, Electrochemical Impedance Spectroscopic Analysis of Dye-Sensitized Solar Cells, J. Phys. Chem. B 109 (2005) 14945–14953.
[40] N. Koide, A. Islam, Y. Chiba, L. Han, Improvement of efficiency of dye-sensitized solar cells based on analysis of equivalent circuit, Journal of Photochemistry and Photobiology A: Chemistry 182 (2006) 296–305.
[41] E. Barsoukov, J.R. Macdonald, Impedance Spectroscopy Theory, Experiment, and Applications, Wiley- Interscience, New Jersey, 2005.
[42] X. Peng, Y. Feng, S. Meng, B. Zhang, Wide frequency range diagnostic impedance behavior of the multiple interfaces charge transport and transfer processes in dye-sensitized solar cells, Electrochimica Acta 88 (2013) 395–403.
[43] M. Adachi, M. Sakamoto, J. Jiu, Y. Ogata, S. Isoda, Determination of Parameters of Electron Transport in Dye-Sensitized Solar Cells Using Electrochemical Impedance Spectroscopy, J. Phys. Chem. B 110 (2006) 13872–13880.